Hydrogen and aromatics recovery through plasma-catalytic pyrolysis of waste polypropylene

Haoyu Xiao [a], Jonathan Harding [b], Shuaishuai Lei [a], Wei Chen [a], Sunwen Xia [a], Ning Cai [a], Chen Xu [a], Junhao Hu [a], Yingquan Chen [a,], Xianhua Wang [a], Xin Tu [b,*], Haiping Yang [a], Hanping Chen [a]*

[a]State Key Laboratory of Coal Combustion, School of Energy and Power Engineering, Huazhong University of Science and Technology, Wuhan, 430074, China

[b]Department of Electrical Engineering and Electronics, University of Liverpool, Liverpool L69 3GJ, UK

[*]Corresponding Authors. E-mail address: chenyingquan@hust.edu.cn (Y. Chen); xin.tu@liverpool.ac.uk (X. Tu)

Abstract:

Plasma-catalysis pyrolysis is a promising way to solve the problem of catalyst deactivation during plastic recycling. In this study, pyrolysis of polypropylene (PP) over zeolite ZSM-5 has been carried out in a two-stage fixed bed pyrolysis system with a coaxial dielectric barrier discharge (DBD) plasma reactor. The role of plasma on the pyrolysis process, as well as the stability of the plasma-catalytic system was investigated. Compared to conventional catalytic pyrolysis, plasma-catalysis pyrolysis increased gas products from 29 wt% to 47 wt% with 4.19 mmol/g H_2 formed, and improved the selectivity of BTX (benzene, toluene, xylene) whilst inhibiting the production of wax simultaneously. After 10 cycles, clear decreases in gas and oil yield (from 86 wt% to 48 wt%) and BTX selectivity (from 71 wt% to 39 wt%) were found in the conventional catalytic pyrolysis, however, nearly no variation was shown in the plasma-catalysis mode. The coupling of catalyst and plasma modified the catalysts acidic sites, while the radicals enhanced the pre-cracking of volatiles, resulting in less deposited coke. Overall, the introduction of plasma resulted in an obvious reduction in total costs and presented a feasible strategy for the recycling of waste plastic.

Keywords: Plastic waste; Catalytic pyrolysis; Plasma enhanced; Hydrogen; Aromatics;

1. Introduction

Global plastic production has increased year on year due to its wide range of applications in many fields. Recently, COVID-19 has aggravated the challenge of plastic pollution, however, this potential threat is greatly overshadowed by the health crisis (Prata et al., 2020). According to the latest report, the epidemic resulted in a monthly global consumption and subsequent waste of approximately 65 billion gloves and 129 billion face masks (Adyel, 2020).

Considering that plastic is derived from fossil fuels, conversion of waste plastic into energy or resources is a promising way to reduce the volume of plastic being released into the environment and conserve the available fossil energy (Oasmaa et al., 2020). Pyrolysis is a highly efficient technology for permanent elimination of plastic and energy recovery (Geyer et al., 2017). However, direct pyrolysis of plastic leads to a wide distribution of products including large amounts of waxes, which may cause blockages along pipelines (Lu et al., 2012). Catalysts can be added to a pyrolysis reactor to convert plastic pyrolysis vapors selectively into high-value products such as chemicals and hydrogen (Weckhuysen, 2020; Yao and Wang, 2020). However, improvement of selectivity and their resistance to deactivation remain as crucial problems for the conversion of plastics into higher-value products using catalysts (Miandad et al., 2016).

A plasma-catalytic pyrolysis system with a plasma zone temperature of 250 °C for biomass conversion was reported by Blanquet et al. (Blanquet et al., 2019). Interestingly, there was less coke deposition on the catalyst compared to non-plasma

66 catalytic processing. Diaz-Silvarrey et al. (Diaz-Silvarrey et al., 2018) found that the
67 amount of ethylene recovered from polyethylene pyrolysis with cold plasma-catalysis
68 (without extra heating) was up to 55 times higher than that obtained in conventional
69 pyrolysis. Liu et al. (Liu et al., 2004) found that the numbers of Bronsted acid sites and
70 Lewis acid sites in the glow discharge plasma-treated Pd/HZSM-5 catalyst were much
71 higher than those found in the untreated catalyst. In addition, plasma has been widely
72 demonstrated in the fields of hydrocarbons cracking (Ahmed et al., 2009), tar reforming
73 (Zhu et al., 2020), as well as solid waste thermochemical conversion (Huang and Tang,
74 2007), showing excellent performance. The effect of combining plasma with catalysis
75 is often greater than the sum of their individual effects, as was reported in some studies
76 (Neyts et al., 2015; Zeng et al., 2018). These show the great potential of introducing
77 plasma to enhance the catalytic pyrolysis of plastic. However, cold plasma-enhanced
78 catalytic pyrolysis as a novel technique has rarely been reported, especially with a high
79 temperature of the plasma zone (with heating). Very little information about the
80 catalytic pyrolysis behavior of plastics with plasma is available, and less attention has
81 been devoted to understanding the role of plasma on the performance and stability of
82 the catalyst.

83 In this study, plasma-catalytic pyrolysis of waste plastic was investigated using waste
84 polypropylene as a typical plastic, with the commercial zeolite ZSM-5 involved as a
85 representative catalyst to facilitate analysis of the mechanism. The influence of plasma
86 power, catalyst amount and catalytic temperature on the reaction performance of the
87 plasma-catalytic pyrolysis were analyzed. Simultaneously, the complex interactions

between plasma, catalyst and volatile were explored to understand the role of plasma. This study was conducted with the aim of providing a better understanding of the catalytic mechanisms for plastic catalytic pyrolysis.

2. Materials and methods

2.1. Materials

The raw plastic waste material used in this study was waste PP collected from disposable lunch boxes. The ultimate analysis was determined using a C/H/N/O elementary analyzer (vario MICRO cube, Elementar, Germany), and the proximate analysis was conducted according to ASTM standards E790, E897 and E830, for moisture, volatiles and ash content, respectively (Yao et al., 2018). The PP contained 85.18 wt% C, 13.74 wt% H and 0.87 wt% O on a dry basis, and proximate analysis of a dry sample indicated that it contained 99.87 wt% volatiles, 0.06 wt% ash, and 0.03 wt% fixed carbon.

Commercial rod-shaped ZSM-5 with a Si/Al ratio of 38 (Surface area ≥ 260 m^2/g, Pore volume ≥ 0.17 cm^3/g) was purchased from the catalyst plant of Nankai University. Prior to each experiment, ZSM-5 was ground and sieved to produce a granular powder with a particle size of 40-60 mesh, and then calcined at 550 ^oC for 5 h in a muffle furnace using air to remove the template residues and moisture in the channels. Before each experiment, the catalyst was dried in an oven at 105 °C for 24 h.

2.2.Plasma-catalytic pyrolysis experiment

As shown in **Fig. 1**, plasma-catalytic pyrolysis of plastic was performed in a two-stage reactor system. The upper stage is a PP thermal-degradation process, while the lower stage is a plasma-catalytic process in a cylindrical DBD plasma reactor. A quartz tube (height: 800 mm, OD: 25 mm and 2.5 mm thickness) was used for both processes. Part of the quartz tube was wrapped with a 100 mm long stainless-steel mesh as a ground electrode, while a 340 mm long ×14 mm OD coaxial stainless-steel pillar was placed in the quartz tube as a high voltage electrode, forming a cold plasma zone between the high voltage electrode and the inner wall of the quartz tube with a gap of 3 mm and a discharge volume of 16 cm^3. A stainless-steel mesh was placed in the middle of the plasma zone and used to support the catalyst. The DBD plasma reactor was connected to an AC high voltage power supply (CTP-2000K, CORONA LAB, Nanjing) with a maximum peak-to-peak voltage of 30 kV and a variable frequency of 5-25 kHz. All the electrical signals were sampled by a two-channel digital oscilloscope (Tektronix TBS1072B, 70 MHz, 1 GS/s).

Before each experiment, a certain amount of ZSM-5 (1, 2, 4 and 6 g) was placed in the plasma zone and the quartz reaction tube was purged with 100 ml/min Argon (99.999%) for 20 min. A heating band was wrapped around the end of the reaction tube to prevent the condensation of products. The input power was kept constant by adjusting the applied voltage and frequency. When the temperature of the upper electric furnace reached 500 ^oC, the PP (2 g) was dropped into the pyrolysis zone and was processed at this temperature for 15 min. The plastic pyrolysis volatiles were carried by the argon (100 ml/min) to the plasma zone for plasma-catalytic pyrolysis. Finally, the

gas products were collected using a gas sampling bag, while the condensable products were condensed. The collected clear liquid we will term oil, and the sticky substance attached to the internal walls of the quartz tube will be referred to as wax. The oil products yield was determined through the weight difference of the coil and pipe condenser, and the gas yield was calculated by combining the volume of all the gases collected during pyrolysis, as explained in our previous work (Chen et al., 2012). The wax yield was calculated by subtraction. In the pyrolysis process, few carbon products (< 3 wt%) were formed on the surface of the catalyst, as such they have no effect on the analysis of the main products even if they are combined with the wax yield. The term "modified catalyst-alone mode" is used when the fresh or spent catalyst had undergone 120 W plasma modification before the catalytic reaction. The sample name method is as shown in the following example: the ratio of ZSM-5 : PP = 2, plasma power = 120 W, catalytic temperature = 400 ^{o}C was defined as 2-120-400. The majority of the experiments were repeated two to three times and marked with error bars.

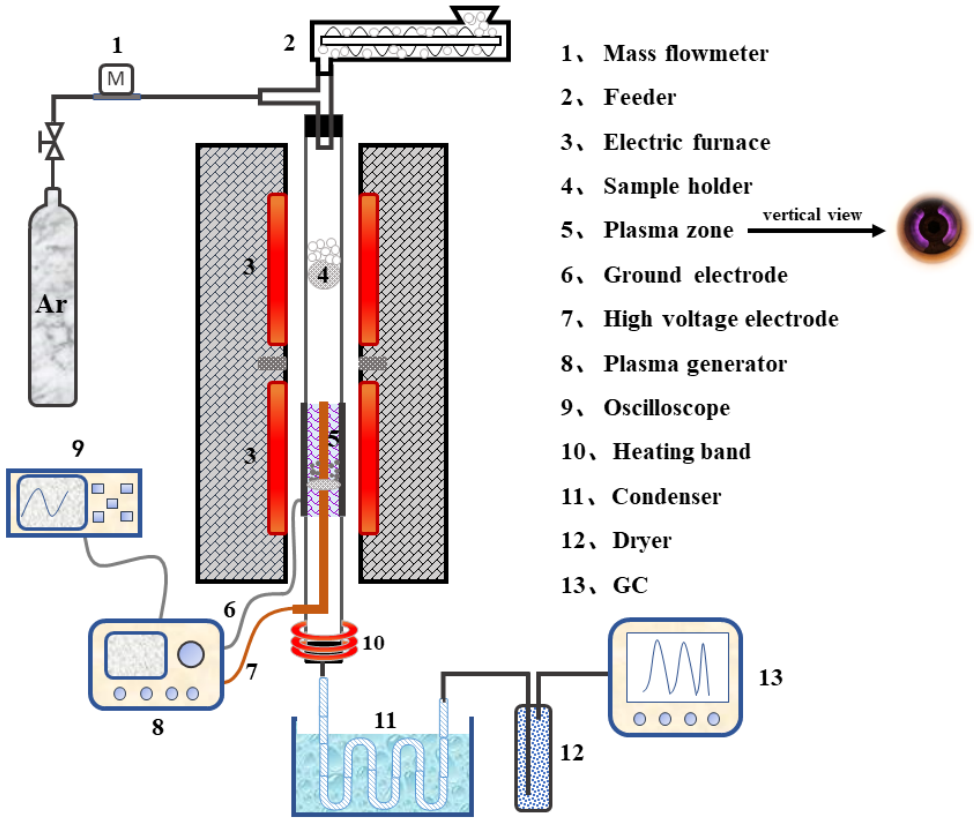

Fig.1. Schematic diagram of the plasma-catalytic pyrolysis of plastic: a two-stage fixed bed system for plasma-catalytic pyrolysis.

2.3. Characterization

2.3.1. Product characterization

The gas products were analyzed using a dual-channel micro-gas chromatograph (Micro-GC 3000A, Agilent Technologies, USA) with thermal conductivity detectors. Two columns were used: Column A (molecular sieve 5A, Ar carrier gas) for analyzing H_2, CO and CH_4 at 95 °C; Column B (ProapakQ-PPQ, He carrier gas) for analyzing CO_2, C_2H_6, C_2H_4, C_2H_2 at 60 °C. Each sample was tested at least three times to take the average.

The liquid products were analyzed using GC–MS (HP7890 series GC with an HP5975 MS detector) with a capillary column (DB-5MS; 30 m×0.25 mm×0.25 um, Agilent). The temperature program was set as follow. It was kept isothermal at 40 °C, then heated to 180 °C at a heating rate of 4 °C/min, it was then heated up to 280 °C at 10 °C/min. Finally, it was kept at 280 °C for 10 min. The flow rate of carrier gas (He) was 1 ml/min, and a 1 μl sample was injected with a split ratio of 80:1. The organic compounds were identified using the Agilent software and the NIST library. Owing to the extremely complex composition of samples, the relative content of each compound was determined by peak area normalization.

2.3.2. Catalyst characterization

The acidity of the zeolite was analyzed using temperature-programmed desorption (TPD) experiments (BELCAT-M, MicrotracBEL Corporation, Japan). A 100.0 mg sample was purged with He and heated from room temperature to 600 °C and maintained there for 60 min. Then, the sample was cooled to 100 °C and purged with NH_3 at 40 mL/min for 60 min. The gas was then switched to He with a flow rate of 40 mL/min and maintained there for 30 min. Finally, the sample was heated to 600 °C at 10 °C/min to desorb NH_3, with the signal recorded from 100 °C. ^{27}Al-NMR and ^{28}Si-NMR analyses were carried out using a solid-state NMR Bruker AVANCE III spectrometer fitted with a 4 mm double resonance probe at a rotation frequency of 14 kHz.

The porous characteristics of the catalysts were measured by N_2 adsorption and desorption with a Quantachrome Autosorb-iQ instrument (USA) to obtain the surface areas, total pore volume, average pore diameter and micropore surface areas of the catalysts based on the Brunauer-Emmett-Teller (BET) method and non-local density functional theory (NLDFT) using adsorption data (Xia et al., 2019). The surface morphologies of the catalysts were obtained using environmental scanning electron microscopy (ESEM; Sigma 300, Carl Zeiss, Germany). The amount of coke deposited on the catalysts was determined with temperature-programmed oxidation (TPO) in a thermogravimetric (TG) analyzer (STA-449F3 NETZSCH, Germany). A sample of 15 mg was heated from room temperature to 800 °C in air (flow rate, 100 mL/min) at a heating rate of 15 °C/min with a holding time of 10 min at 105 °C and 800 °C.

3. Result and discussion

3.1. Plasma-catalytic pyrolysis of PP

The effect of plasma power, catalyst ratio and catalytic temperature on the plasma-catalysis pyrolysis of PP was firstly investigated. The yield distribution and product composition at various plasma powers are shown in **Fig. 2a**. Without plasma, catalytic pyrolysis of PP produced large amounts of oil (54 wt%) with some gas (20 wt%) and lots of wax (26 wt%) stuck to the inner wall of the reactor. These waxes were mainly paraffinic (> C_{20}) with a melting point of 70 °C (Lopez et al., 2017). When switching on the plasma (60 W), the gas yield increased rapidly and the wax yield decreased significantly, while the oil yield only slightly decreased. Increasing plasma power

decreased the yield of gas products and wax but did not change the oil yield. At a plasma power of 120 W, the wax was almost eliminated. These findings suggest that plasma promotes the cracking of heavy hydrocarbons to light hydrocarbons.

As shown in **Fig. 2b**, C_3H_8 was the main component of the pyrolysis gas, and H_2 was not detected for the pyrolysis of PP without plasma, this suggests that it is difficult to break C–H bonds at a catalysis temperature of 400 °C. After switching on the plasma (60 W), the volume percent of C_3H_8 decreased from 75% to 50%, while the volume of H_2 and CH_4 increased by 18% and 7%, respectively. This phenomenon implies that plasma facilitated the cleavage of C–H and C–C bonds. Further increasing the plasma power increased the content of H_2 and CH_4 but decreased the formation of C_3H_8. The volume content of H_2 and CH_4 reached a maximum of 23% and 18%, respectively at 120 W.

In the absence of the plasma, the oil products mainly contained benzene, toluene and xylene due to the catalytic effect of ZSM-5 (**Fig. 2c**). Introducing plasma to this process (60 W) slightly increased the formation of benzene and toluene but reduced the content of xylene. Upon increasing plasma power, the xylene content further decreased, while the benzene content increased until the power reached 80 W, the toluene content began to ascend rapidly when the power was higher than 80 W. These results suggest that plasma promoted the cleavage of the methyl group of xylenes, producing more toluene and benzene. The formation of other aromatics such as naphthalene decreased when increasing the plasma power, indicating that plasma promoted the conversion of other

222 aromatics to BTX. Interestingly, the production of non-aromatics was almost
223 unaffected by increasing the plasma power.

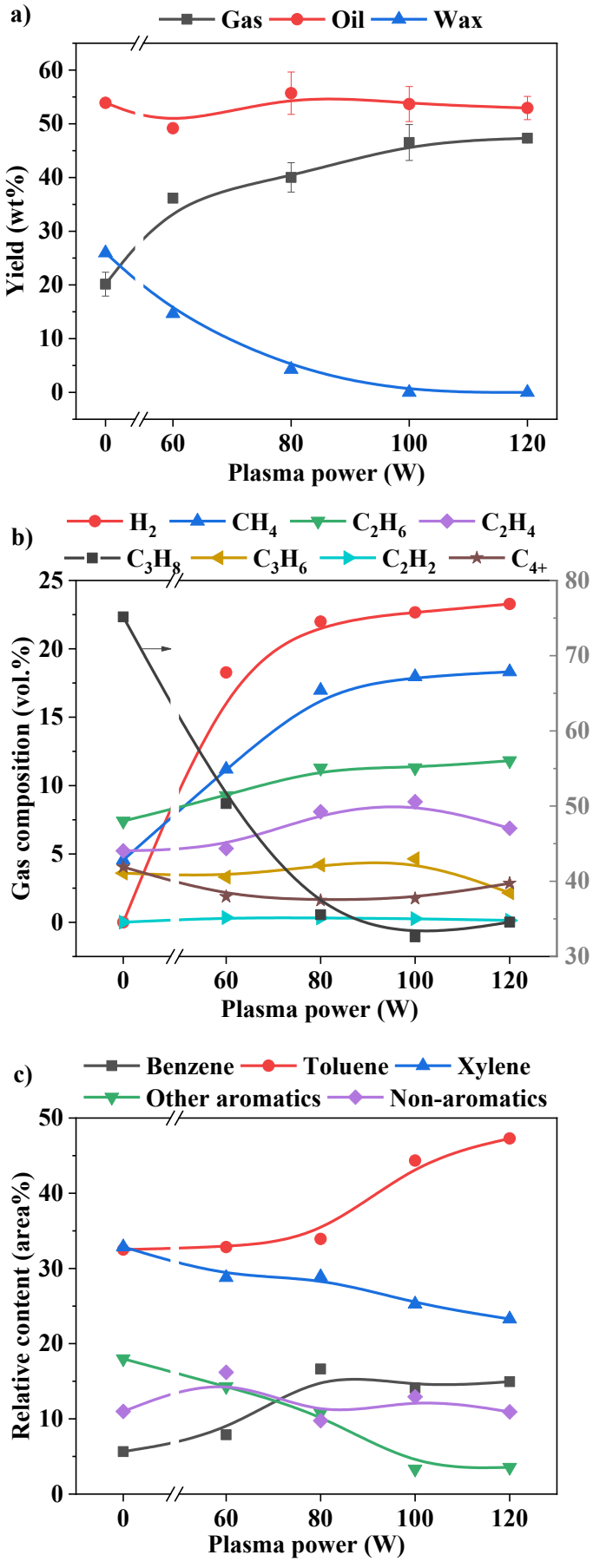
a)
Gas
Oil
Wax
Yield (wt%)
Plasma power (W)
b)
H2
CH4
C2H6
C2H4
C3H8
C3H6
C2H2
C4+
Gas composition (vol.%)
Plasma power (W)
c)
Benzene
Toluene
Xylene
Other aromatics
Non-aromatics
Relative content (area%)
Plasma power (W)

Fig. 2. Influence of plasma power (at ZSM-5/PP mass ratio = 2 and 400 °C) on a) product distribution, b) gas and c) oil compositions of PP plastic pyrolysis.

Fig. 3a shows the influence of the catalyst ratio on the plasma-catalytic pyrolysis of PP. Without a catalyst, the main product was wax (60%), while some liquid oil and limited gas products also formed. Increasing the catalyst amount significantly enhanced the yield of gas and oil products and reduced the formation of wax. The maximum yield of oil and gas products was attained at a Z/P (ZSM-5/PP) ratio of 3 when the wax has almost disappeared. These results indicate that ZSM-5 can enhance the decomposition of wax into oil and gas.

As shown in **Fig. 3b**, in the absence of a catalyst, H_2 and CH_4 account for 72 vol.% of the gas composition. Increasing the Z/P ratio from 0 to 1 considerably enhanced the production of H_2 and CH_4 but significantly reduced the formation of C_3H_8 and C_2H_4. Further increasing the Z/P ratio from 1 to 3 does not show any obvious variation of the gas products except C_3H_8. This finding indicates the formation of C_3H_8 is directly related to the catalyst, and the β-scission step was dominant in the presence of ZSM-5 (Vogt and Weckhuysen, 2015).

Fig. 3c shows the GC/MS peak areas (%) of the oil compositions from the plasma-catalytic pyrolysis of plastics. Without a catalyst, nearly 90% of the oil was nonaromatic (**Fig. S2**). The addition of the catalyst directly increased the BTX content by almost 70%, indicating ZSM-5 played a critical role in improving the selectivity of aromatic products in the plasma-catalytic process. Increasing the catalyst amount did not change

247 the BTX content but the content of aromatics increased when the Z/P ratio > 1. This
248 might be due to excessive catalysts promoting further aromatization for other aromatics
249 such as naphthalene.

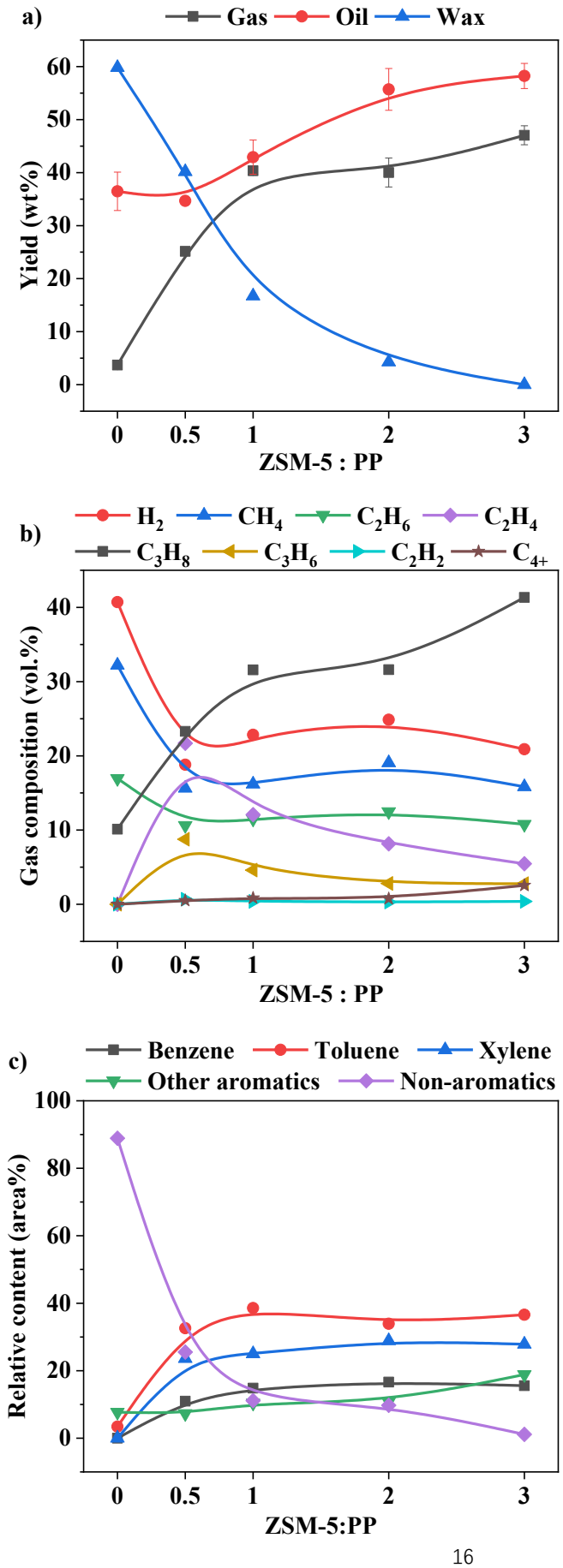
a)
Gas
Oil
Wax
Yield (wt%)
ZSM-5 : PP
b)
H2
CH4
C2H6
C2H4
C3H8
C3H6
C2H2
C4+
Gas composition (vol.%)
ZSM-5 : PP
c)
Benzene
Toluene
Xylene
Other aromatics
Non-aromatics
Relative content (area%)
ZSM-5:PP

Fig. 3. Influence of the ZSM-5/PP mass ratio (at 80 W and 400 °C) on a) product distribution, b) gas and c) oil compositions of PP plastic pyrolysis.

Fig. 4a shows the variation of pyrolysis products at different catalytic temperatures. At a temperature of 200 °C, the yield of wax and gas reached nearly 30 wt.% and 19 wt.%, respectively (see **Fig. 4a**), while the main product (oil) accounted for 51 wt.%. Upon increasing the catalytic temperature, the yield of wax decreased drastically, and almost no wax was found at 500 °C. In contrast, increasing the temperature of the catalyst bed enhanced the gas yield significantly but slightly decreased the generation of oil products.

As shown in **Fig. 4b**, C_3H_8 and H_2 were the main gas products at a low temperature (200 °C). Increasing the catalytic temperature enhanced the production of almost all gas products except C_3H_8 and C_{4+}. The volume content of C_3H_8 dropped significantly with the increase of the catalyst temperature. Propylene can be mainly formed via chain-end scission (Kruse et al., 2003), and formed earlier when a catalyst surface was provided (Vollmer et al., 2021), thus the amount of propylene was supposed to increase. The reduction indicated that propylene was the key reactant for catalysis, while hydrogen and methane were products.

At 200 °C, the oil products had a high content of toluene and xylene and a relatively low content of benzene (**Fig. 4c**). Increasing the temperature reduced the content of xylene and enhanced the formation of benzene. By contrast, the content of toluene dropped first and then increased when varying the temperature from 200 to 500 °C.

These results could be ascribed to the high temperature promoting the cleavage of methyl bonds on xylene. This finding is similar to those presented in **Fig. 2c**. Interestingly, the BTX selectivity was almost independent of the temperature but increased when increasing the plasma power, suggesting that the performance of the ZSM-5 catalyst was enhanced due to the modification of the catalyst by plasma.

The results presented in Figs. 2-4 clearly indicate that the increase of plasma power, catalyst amount and temperature reduces the formation of wax whilst generating more gas and oil products. PP can be completely converted into gas and oil products at a plasma power of 100 W, a Z/P ratio of 2 and a temperature of 400 ^{o}C.

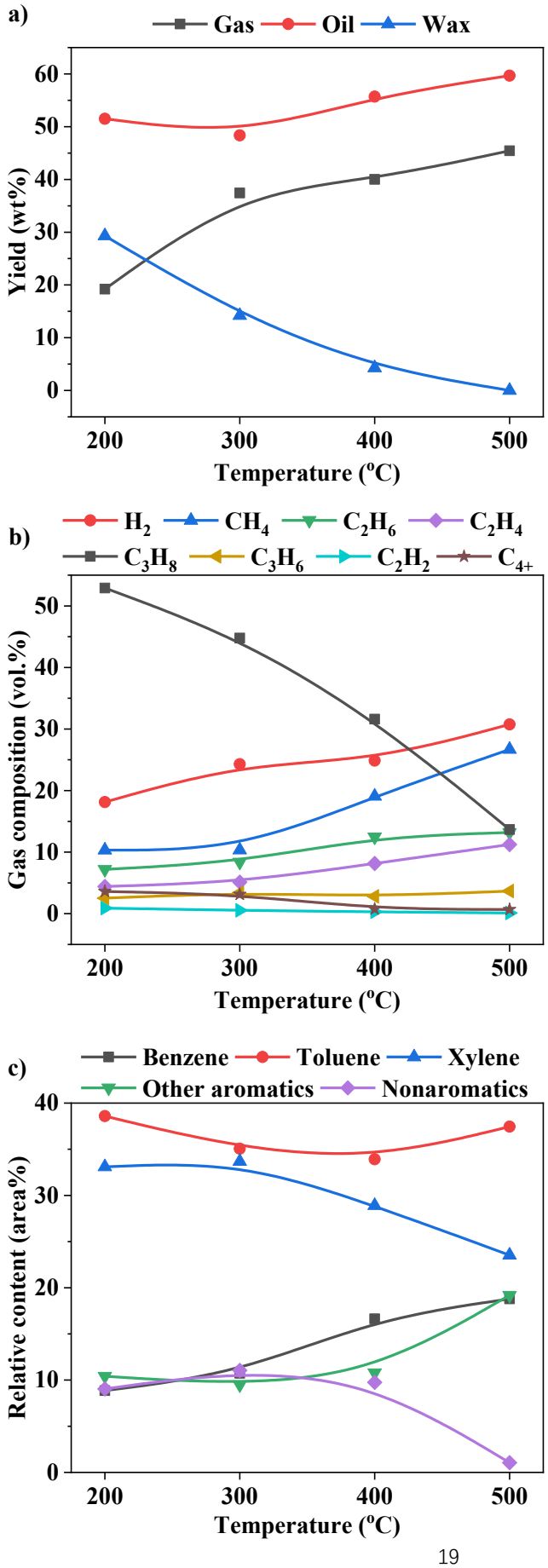
a)
Gas
Oil
Wax
Yield (wt%)
Temperature (°C)
b)
H2
CH4
C2H6
C2H4
C3H8
C3H6
C2H2
C4+
Gas composition (vol.%)
Temperature (°C)
c)
Benzene
Toluene
Xylene
Other aromatics
Nonaromatics
Relative content (area%)
Temperature (°C)

Fig. 4 Influence of temperature (at Z/P mass ratio = 2 and 80 W) on a) product distribution, b) gas and c) oil compositions of PP pyrolysis.

3.2. The role of plasma in the catalytic pyrolysis process

Five different pyrolysis process modes: direct pyrolysis (0-0-400), plasma-alone pyrolysis (0-120-400), catalyst-alone pyrolysis (2-0-400), modified catalyst-alone pyrolysis (catalyst modified by 120 W plasma before catalysis reaction, 2-0-400) and plasma-catalysis pyrolysis (2-120-400) were compared to get a better understanding of the synergistic effect of plasma catalysis and pyrolysis.

As shown in Fig. 5, the direct pyrolysis of PP produced 2 wt.% gas, 44 wt.% oil and a large amount of wax (54 wt.%). This very small amount of gas released included CH_4, C_2H_6, C_2H_4 and C_3H_8. A large number of cycloparaffins (59%) and olefins (27%), as well as a small number of aromatics (6%), were also produced (see Table S1). The composition of the products is similar to that reported in previous studies (Aguado et al., 2002; Muhammad et al., 2015).

Introducing plasma into the pyrolysis process considerably enhanced the gas yield (nearly 22 wt.%) and greatly decreased the generation of wax products from 54 wt% to 31 wt%, this indicates that plasma-enhanced the decomposition of waxes into light gas products even without a catalyst. All the gas products increased significantly, suggesting that plasma does not favor selective scission of PP and the reaction intermediates. Active species such as metastable Ar species and electrons collide with volatiles to form carbenium-like ions, the β-scission reaction can occur where the C–C

bond between the beta carbon (i.e. the one next to the carbocation) and the following one is broken, resulting in a smaller carbocation and a shorter olefin (Diaz-Silvarrey et al., 2018). No obvious variation of aromatics was observed with the assistance of plasma, but the content of olefins increased to 73% while the content of cycloparaffins decreased to 9% (see **Table S2**). This might be due to plasma causing the C–H and C–C bonds to break, resulting in the formation of unsaturated bonds and hydrogen ions which is consistent with the observations shown in the gas compositions.

The presence of ZSM-5 was particularly efficient for wax removal, but nearly 17 wt% wax was still left on the cold pipe. The gas and oil yields were also relatively higher than the plasma-alone mode. Compared to the previous two modes, it was clear that the catalyst-alone mode increased the amount of C_3H_8 and C_{4+} significantly, and the absence of H_2 indicates that the formation of H_2 might be driven by the plasma. In addition, the plasma-alone mode produced an overall lighter gas than the catalyst-alone mode. As for oil composition, the BTX selectivity reached over 70%, while the content of toluene and xylene was more than 30%, respectively.

After the catalyst was modified by the plasma (at 120 W), the distribution of products obtained in the modified catalyst-alone mode evolved similarly to that obtained under the original catalyst-alone mode. Compared to the catalyst-alone mode, the presence of ZSM-5 further reduced wax to around 8 wt.% and increased the oil yield by 6 wt.%, while the gas yield only slightly increased. The gas produced had more C_3H_8 and C_{4+}, and the oil products showed a higher benzene, toluene and xylene content than that without plasma modification. These results indicate that plasma modification might

enhance the catalytic activity of ZSM-5 and the stronger catalytic activity of ZSM-5 was more conducive for promoting oil production (Liu et al., 2004; Yaneva et al., 2016).

In the plasma-catalysis mode, it is noteworthy that all waxes were almost eliminated with a significant increase in the gas yield. López et al. (Lopez-Urionabarrenechea et al., 2011) reported that 400 °C is not high enough to decompose plastics, since a solid residue (unconverted plastic) near 30 wt% was obtained in the ZSM-5 catalytic experiments. This highlights the advantage of plasma-catalysis pyrolysis. The amount of H_2, CH_4, C_2H_6, C_2H_4 and C_3H_8 showed explosive growth compared to the plasma-alone and catalyst-alone modes, indicating a significant synergistic effect between the plasma and catalyst. The content of benzene increased from 6% to 15%, and the toluene content also increased by 14%, compared to the catalyst-alone mode. On the contrary, the content of xylene dropped from 33% to 23%. These findings suggest the plasma promoted the breaking of the methyl bond on xylene generating toluene and benzene. The broken methyl groups combined with hydrogen ions from the broken C–H bond to form CH_4, this is supported by the results of the gas composition in **Fig. 5b**.

Comparing these five modes, it was obvious that the production of H_2, CH_4, C_2H_6 and C_2H_4 is closely related to the presence of plasma, while the formation of C_3H_8 is related to the presence of ZSM-5. The plasma catalysis provided a more reactive environment with more energetic species, increasing the formation of carbocations and radicals in the hydrocarbon chains and enhancing the cleavage of C–C and C–H bonds and therefore promoting the formation of light hydrocarbons and H_2. In the meantime, the exposure of the catalyst to the plasma would modify the catalysts morphology, acidic

sites and oxidation state (Guo et al., 2006; Liu et al., 2004), leading to stronger catalyst activity. Zhang et al (Zhang et al., 2015). investigated the microwave pyrolysis of LDPE with a ZSM-5 catalyst and found that the highest yield of oil was 32.58 wt.%, whereas 65.13 wt% gas was obtained. The mono-ring aromatic hydrocarbons were detected in abundance in the upgraded pyrolysis oils at 74.73–88.49%. However, the reaction temperature (480 °C) and microwave power (700 W) were much high than the conditions used in this work. Compared with conventional catalytic pyrolysis, novel pyrolysis methods, such as plasma and microwave, can improve gas yield and oil selectivity. The pros and cons of these two methods are worthy of further comparison.

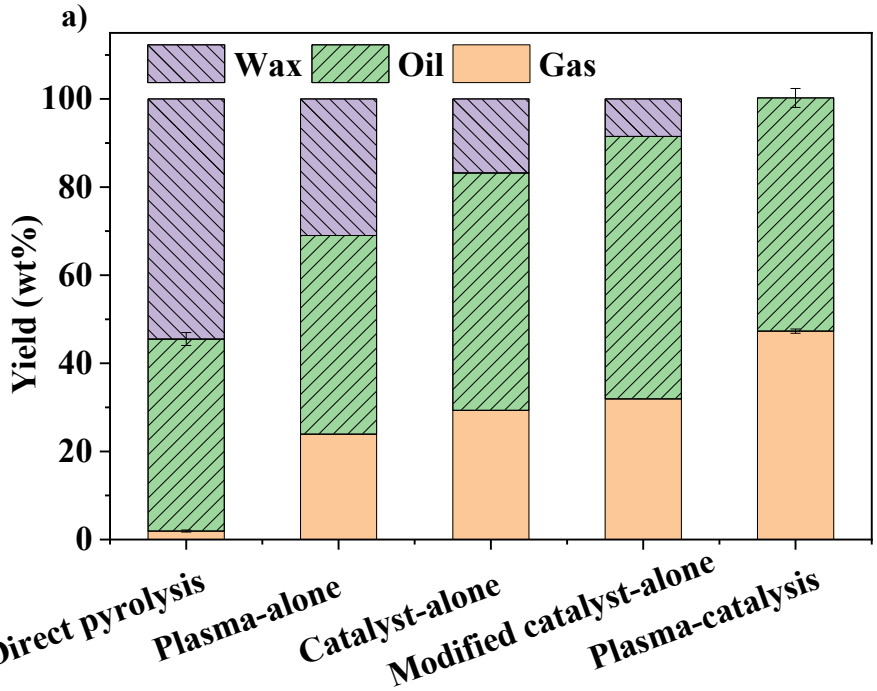

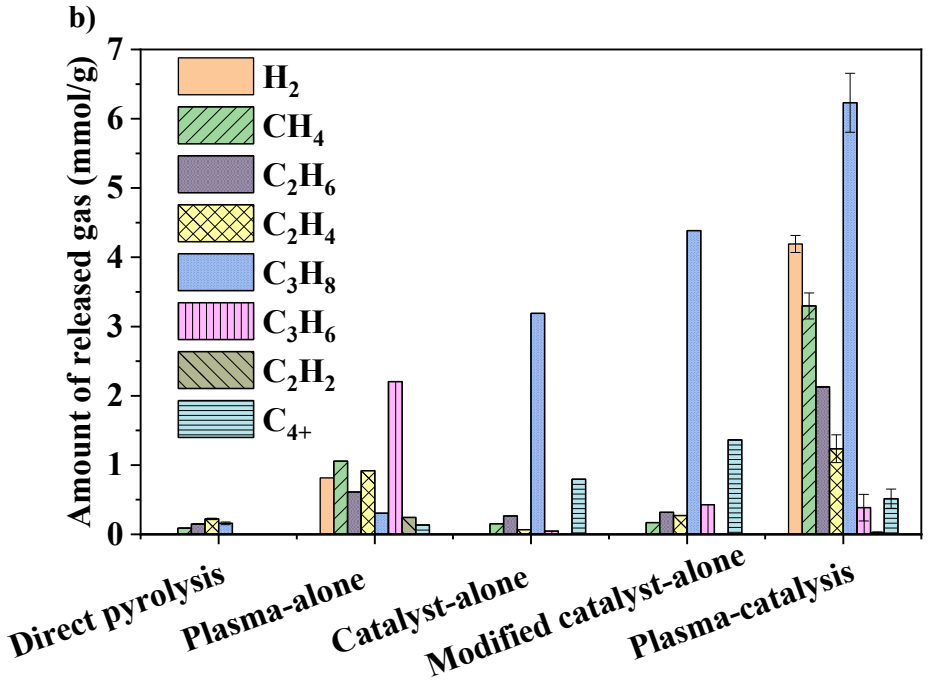

359

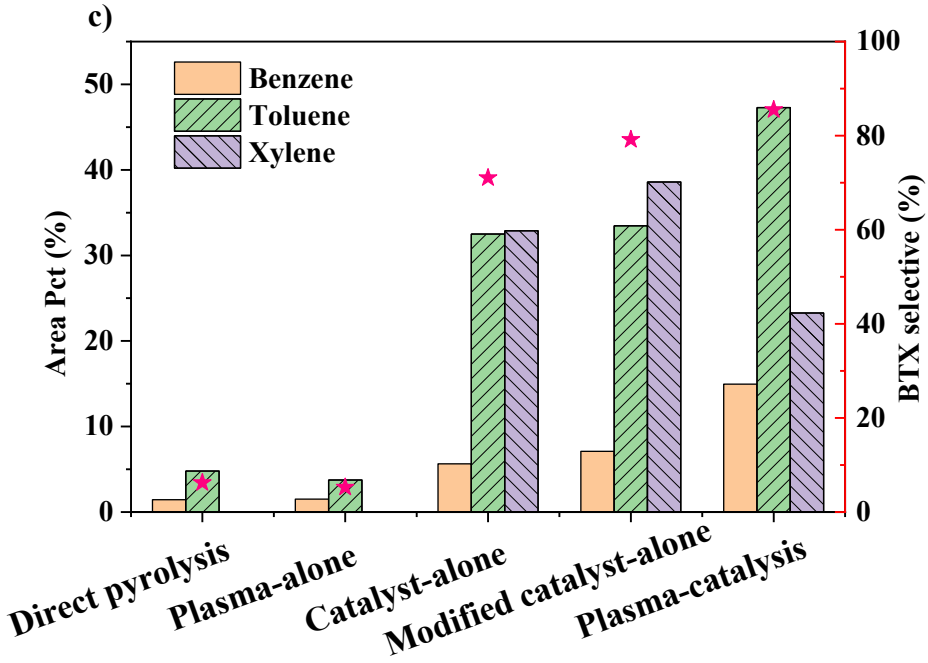

360

361 **Fig. 5.** Influence of plasma and catalyst on the products distribution, gas and oil

362 compositions of PP pyrolysis.

363

In this work, the distribution of the products could be associated with the acidity of the catalysts determined by NH_3-TPD. As shown in **Fig. 6**, the ZSM-5 catalyst has a typical TPD profile of zeolite which consists of two main desorption peaks (Che et al., 2019). Compared to the fresh ZSM-5, the TCD signal of the catalyst modified by the plasma was much stronger, indicating that plasma modification increased the number of acid sites on the ZSM-5 catalyst. This phenomenon can be attributed to the breakdown of siloxane bonds and the formation of new hydroxyl groups (Si–OH and Al–OH) on the zeolite edges induced by reactive species created by the plasma (Yaneva et al., 2016). After the reaction using the catalyst-alone mode, the number of acid sites of the spent ZSM-5 catalyst significant decreased, suggesting that coke deposition covered the acidic sites on the catalyst surface. In the modified catalyst-alone mode, the number of acidic sites of the modified ZSM-5 decreased after the reaction, but it was still approximate to that of the fresh ZSM-5 catalyst without plasma modification. For the plasma-catalysis mode, the number of acidic sites on the catalyst was still higher than that of the fresh ZSM-5 and slightly lower than that of the modified ZSM-5 catalyst. This finding might be attributed to the increased number of acidic sites produced and the reduction in coke formation due to plasma modification (Blanquet et al., 2019).

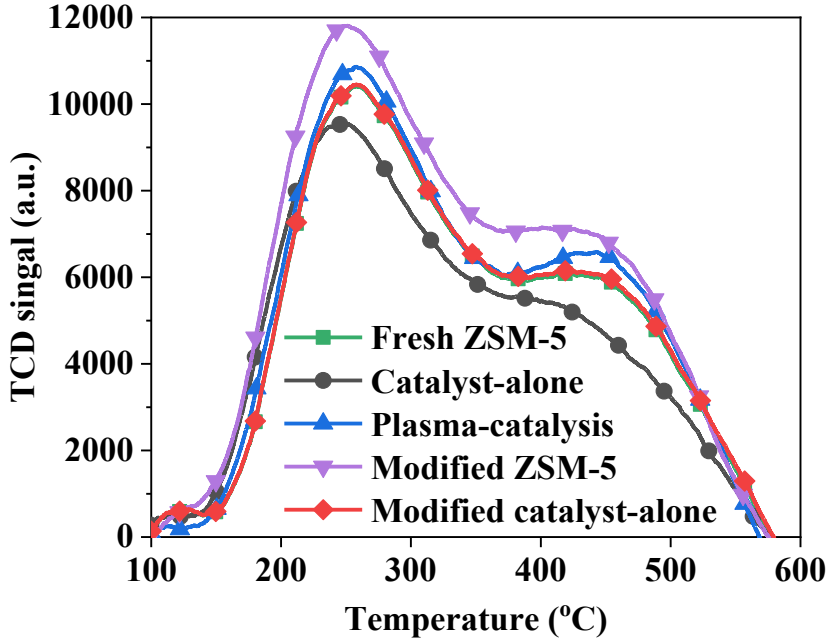

382

383 **Fig. 6.** NH_3-TPD profiles of fresh ZSM-5, modified ZSM-5 and spent ZSM-5.

384

385 **3.3. Effect of plasma on the stability of the catalyst**

386 **3.3.1.** Catalyst stability test

387 **Fig. 7** shows a stability study of ZSM-5 for the catalyst-alone, modified catalyst-
388 alone and plasma-catalysis modes. After 10 cycles, remarkable reductions in gas and
389 oil yield (86 wt% to 48 wt %), BTX selectivity (71% to 39%) and the amount of C_3H_8
390 were observed for the catalyst-alone mode, indicating significant catalyst deactivation.
391 For the modified catalyst-alone mode, the reduction in gas and oil yield and BTX
392 selectivity were relatively low. The results suggest that parts of the wax on the catalyst
393 surface can be decomposed by the bombardment of energetic species, resulting in
394 deactivation being alleviated (Ahmed et al., 2009). However, it is worth noting that no
395 obvious variation of the gas and oil yield, BTX selectivity and the amount of produced

396 C_3H_8 were found in the plasma-catalysis mode, indicating that the plasma-catalysis
397 system showed excellent stability. Plasma-catalysis can produce less deposited coke
398 compared to non-plasma catalytic processing (Blanquet et al., 2019). The absence of
399 H_2 production from the catalyst-alone and modified catalyst-alone modes reveals that
400 the formation of H_2 is mainly related to plasma cracking of hydrocarbons. However,
401 the amount of H_2 decreased with the increase of the reaction cycle, which may be related
402 to a reduction of its precursor caused by a slightly reduced catalyst performance.
403 Moreover, the downward trend shown for the catalyst-alone mode was relatively
404 sharp at the beginning of the cycle, before becoming relatively retardatory towards the
405 end of the cycle, however, the deactivation rate for the modified catalyst-alone mode
406 was more linear. These results show that the catalyst deactivation rate is faster in the
407 first half of the cycle than that in the second half of the cycle for the catalyst-alone
408 mode. It could be speculated that some wax deposition blocked the pores on the catalyst
409 surface, making it difficult for heavy volatiles to enter the internals of the catalyst. As
410 a result, a more rapid catalyst deactivation happened in the first few cycles, with only
411 lighter volatiles able to enter the internal pores for catalytic reactions in the subsequent
412 cycles. In contrast, the deactivation rate of the modified catalyst is relatively uniform,
413 which may be attributed to the plasma's cleaning effect on wax formed on the catalyst
414 surface (Ahmed et al., 2009).

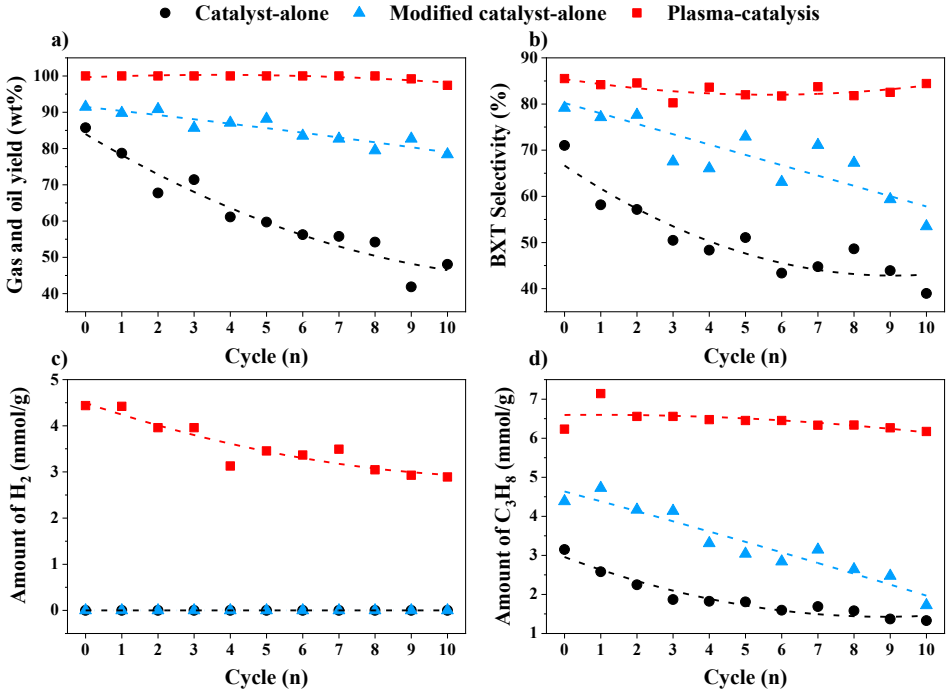

415

416 **Fig. 7.** Stability tests for the catalyst undergoing catalyst-alone pyrolysis and plasma-

417 catalysis pyrolysis.

418

419 **3.3.2.** Effect of plasma on the catalyst

420 **Fig. 8** compares the acidity of the catalysts in two modes after 10 reaction cycles. To

421 get more detailed information about the change of acidity of the catalysts after 10

422 reaction cycles, each curve was divided into three peaks according to the method in the

423 literature (Zheng et al., 2014). The peaks centered at around 180–220 °C, 230–310 °C

424 and 360–450 °C correspond to the desorption of NH_3 for the weak acid, medium acid

425 and strong acid positions, respectively. Clearly, the catalyst used in the plasma-catalysis

426 mode contained more medium and strong acid sites and fewer weak acid sites,

427 highlighting that the presence of the plasma enhances the formation of strong and

428 medium acid sites on the catalyst surface during the catalytic process (Kwak et al.,

2006). The enhanced formation of strong acid sites also explains why the plasma-catalysis had a better catalytic performance at 400 °C than conventional catalytic pyrolysis.

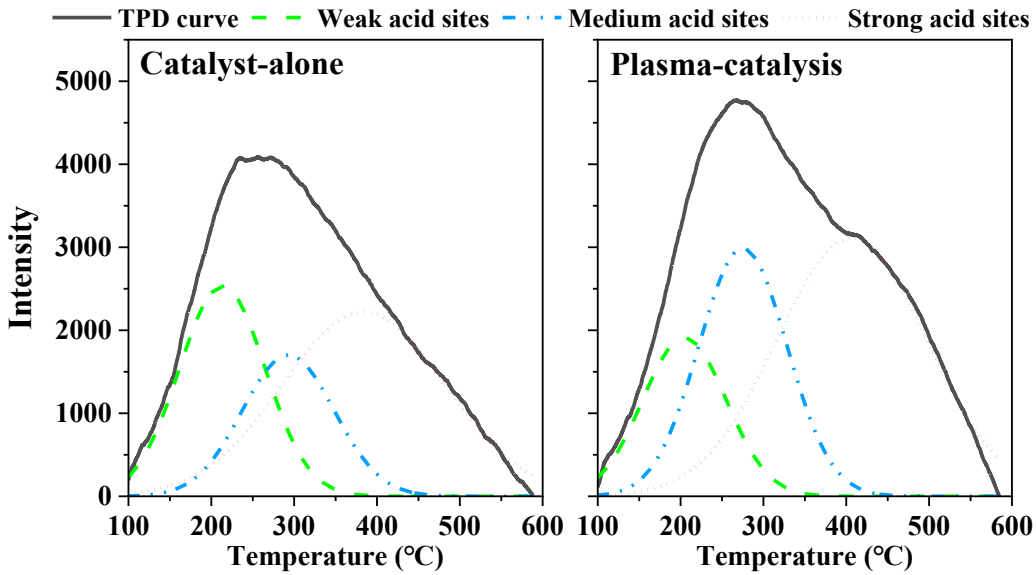

Fig. 8. NH_3-TPD profiles of spent ZSM-5 after 10 reaction cycles under catalysis-alone pyrolysis and plasma-catalysis pyrolysis.

To achieve a better understanding of the plasma modification on the ZSM-5 catalyst, further ^{27}Al and ^{29}Si -NMR analysis was performed to determine the location of Al in the structure. As shown in **Fig. 9**, the fresh ZSM-5 catalysts and plasma modified ZSM-5 showed the same chemical shift and resonance in both ^{27}Al and ^{29}Si -NMR spectra, suggesting plasma modification had no effect on the silicon-aluminum structure of the zeolite. **Fig. 9a** shows the ^{27}Al-NMR spectra of a spent ZSM-5 after 10 cycles. A predominant peak located at about 0 ppm is ascribed to octahedral Al coordination which is described as extra-framework aluminum (Ravi et al., 2020). Another peak of tetrahedral framework aluminum with a chemical shift at around 50 ppm was observed.

Obviously, the peak intensity of tetrahedral framework aluminum and octahedral Al coordination increased significantly after the reaction, and the spent catalyst used for plasma-catalysis exhibited the highest peak intensity. The ^{29}Si-NMR spectrum in **Fig. 9b** presented a broad peak with a chemical shift around 95 ppm assigned to Si(2Al) and a small peak located at about -89 ppm assigned to Si(3Al), suggesting limited aluminum species in the vicinity of Si atoms which is in agreement with ^{27}Al- NMR spectrum. The presence of broad ^{29}Si typical peaks of zeolites might be due to impurities on the catalyst and broad distribution of coordinated Si sites, with different extents of cross-linking and non-uniform Si–O–Si bond angles or bond distances (Epping and Chmelka, 2006; Lippmaa et al., 1981). After the reaction, the broad peak intensity reduced and the small peak disappeared, indicating reduced aluminum content in the framework. Compared to the spent catalyst used for plasma-catalysis, the catalyst after the catalyst-alone reaction exhibited a lower peak intensity, suggesting its lower aluminum content. These NMR results provide a possible explanation for the low acidity of the catalyst in the catalyst-alone mode.

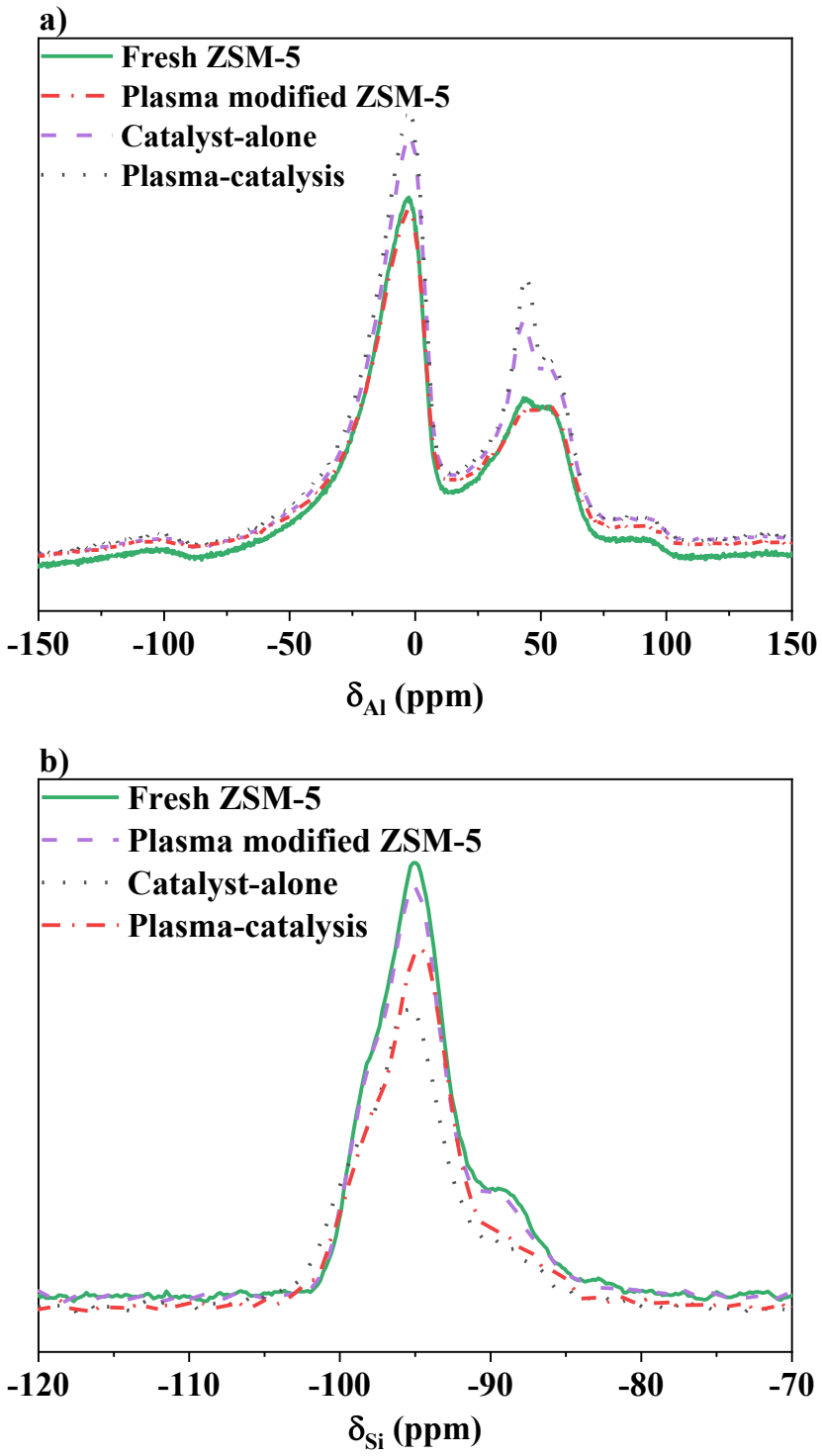

Fig 9. ^{27}Al-NMR spectra and ^{29}Si-NMR spectra of spent ZSM-5 after 10 cycles under catalysis-alone pyrolysis and plasma-catalysis pyrolysis.

Temperature programmed oxidation (TPO) was used to investigate the coke deposition on the spent catalysts. As shown in **Fig. 10**, the derivative weight loss thermograms exhibited two distinct peaks at temperatures around 180 and 580 °C, respectively. Therefore, the oxidation process involved two main stages: the removal of water in the range of 100–250 °C and the coke combustion from 250 °C to 700 °C. Clearly, the weight loss of coke is dominant, and plasma-catalysis produced less deposited coke compared to the non-plasma catalytic process. It is noteworthy that the presence of the plasma increased the number of acid sites of the catalyst and promoted the cleavage of the C-H bond, which can promote cyclization and polymerization due to the dehydrogenation of hydroaromatic and expansion of the skeletal carbon network (Xia et al., 2022). These results indicate a complex mechanism of coke formation in the plasma-catalytic pyrolysis of PP. Blanquet et al. (Blanquet et al., 2019; Kameshima et al., 2015) speculated that the contribution of the Boudouard reaction to plasma-catalysis leads to less deposited coke compared to catalysis-alone. It is clear that the catalyst used for catalyst-alone showed a much higher derivative weight loss rate in the range of 250 °C to 400 °C, which may be explained by the degradation of paraffin wax (George et al., 2020). This finding indicates that plasma-catalysis can also inhibit the adhesion of wax on the catalyst. In addition, reactive species formed in the plasma promoted the decomposition of long-chain hydrocarbons to short-chain hydrocarbons (Deminsky et al., 2002).

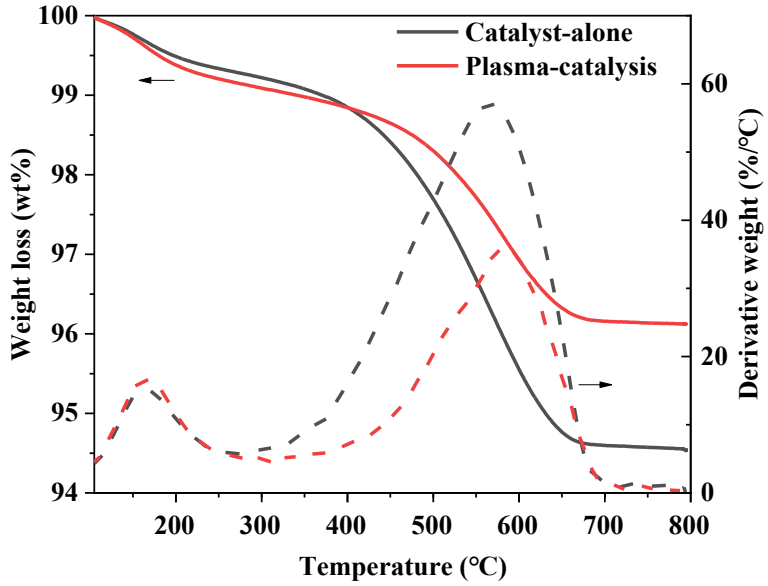

Fig. 10. Temperature programmed oxidation of spent ZSM-5 after 10 cycles under catalysis-alone pyrolysis and plasma-catalysis pyrolysis.

Table 1 The pore characterizations of the catalyst

	Surface area (m^2/g)	Micropore area (m^2/g)	Total pore volume (cc/g)	Average pore diameter (nm)
ZSM-5	323.04	235.84	0.31	3.85
PMZ	323.82	237.72	0.31	3.80
CA10	147.76	34.22	0.19	5.34
PC10	250.84	133.50	0.24	3.83

Note: PMZ, CA10 and PC10 represent plasma modified ZSM-5, the ZMS-5 at catalyst-alone mode after 10 cycles, the ZSM-5 at plasma-catalysis mode after 10 cycles.

494 The pore size distribution of fresh, modified and spent catalysts after 10 reaction
495 cycles is listed in **Table 1**. For ZSM-5, the BET surface area, micropore area, total pore
496 volume and average pore diameter was 323.04 m^2/g, 235.84 m^2/g, 0.31 cc/g and 3.85
497 nm, respectively. Plasma modification of the ZSM-5 catalyst did not change its surface
498 area, micropore area, total pore volume and average pore diameter, revealing that
499 plasma modification does not change the physical pore structure of the catalyst.
500 Compared to the fresh ZSM-5, the surface area, micropore area and total pore volume
501 of the spent catalysts after 10 cycles reaction decreased significantly, this is especially
502 true for the spent catalyst which was used in the catalyst-alone mode, which can be
503 ascribed to deposited wax and the coke blockage in the pores of the catalyst. Notably,
504 the micropore area of the spent catalyst used in the catalyst-alone mode was reduced
505 drastically from 235.84 m^2/g to 34.22 m^2/g, compared to that used in the plasma-
506 catalysis mode which dropped to 133.50 m^2/g. The external pores of the catalysts were
507 blocked by the deposited wax and coke, thus the internal micropores cannot be detected.
508 By contrast, the spent catalysts after the plasma-catalytic reaction showed a similar
509 average pore diameter with the fresh ZSM-5, which indicates that the wax and coke
510 were uniformly deposited across the surface in pores of varying sizes.
511 The surface morphologies of the fresh ZSM-5 and spent ZSM-5 catalysts after 10
512 reaction cycles were determined by SEM analysis, as shown in **Fig. 11**. The fresh ZSM-
513 5 surface was relatively flat and smooth with a flaky texture and became rougher after
514 plasma modification. Many coral-like substances were attached to the surface of the
515 spent catalyst after the catalyst-alone process, while very small amounts of

agglomerated particles were tightly attached to the surface and pores of the spent catalyst after the plasma-catalytic reaction. Polypropylene has a rather low molecular weight ($M_w \approx 12000$ g/mol), while the root-mean-square end-to-end distance in its coiled state is about 9 nm and the average length of the fully extended polymer is 73 nm. As a result, the chains are suspected not to be able to enter deep into the zeolite pores (0.7 nm) without pre-cracking (Vollmer et al., 2021). This suggests that non-plasma catalysis tended to form dense agglomerates on the catalyst surface blocking pores, while plasma-catalysis provides some pre-cracking allowing the reactants to enter deep into the complex pore network of the catalyst more easily and thus be aromatized further.

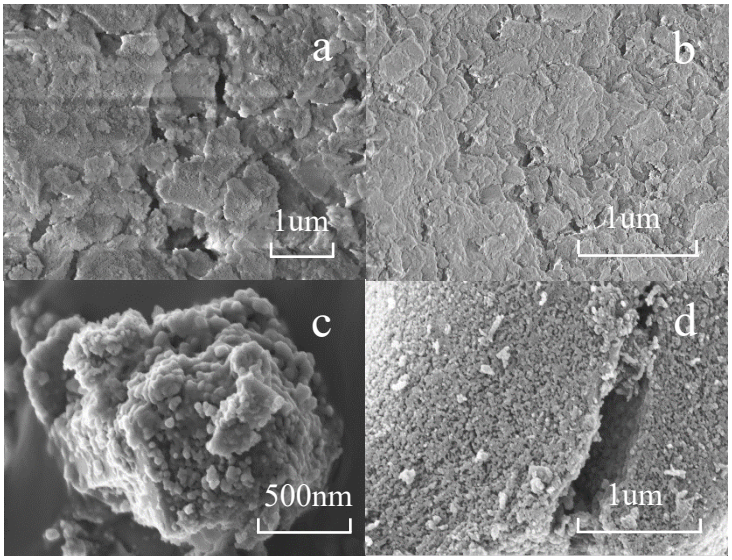

Fig. 11. SEM images of (a) fresh ZSM-5, (b) plasma modified ZSM-5 and spent ZSM-5 after 10 cycles under (c) catalyst-alone pyrolysis and (d) plasma-catalysis pyrolysis.

As shown in Fig. 12, large amounts of heavy hydrocarbon intermediates have difficulty entering the internal micropores of the catalyst during the catalyst-alone

pyrolysis, resulting in the blockage of the catalyst pores due to coke deposition. The aromatization was limited due to inaccessible acid sites on the catalyst. In comparison, plasma-enhanced the pre-cracking of heavy intermediates into light intermediates which can diffuse into the internal pores of ZSM-5. The synergistic effect from the combination of plasma with catalysis during the pyrolysis process can be divided into the effect of plasma on volatiles and the modification of the catalyst by the plasma. On the one hand, plasma can produce highly energetic electrons which have higher energies than the bond dissociation energies of PP (C–H = 415 kJ/mol and C–C = 331 kJ/mol) and therefore promote pre-cracking (Diaz-Silvarrey et al., 2018). On the other hand, plasma can change the acid sites and defects formed on the catalyst surface, enhancing the performance of the catalyst. Plasma-catalytic pyrolysis has shown promising potential for dealing with the challenges in the conversion and utilization of plastics such as catalyst deactivation and low product quality.

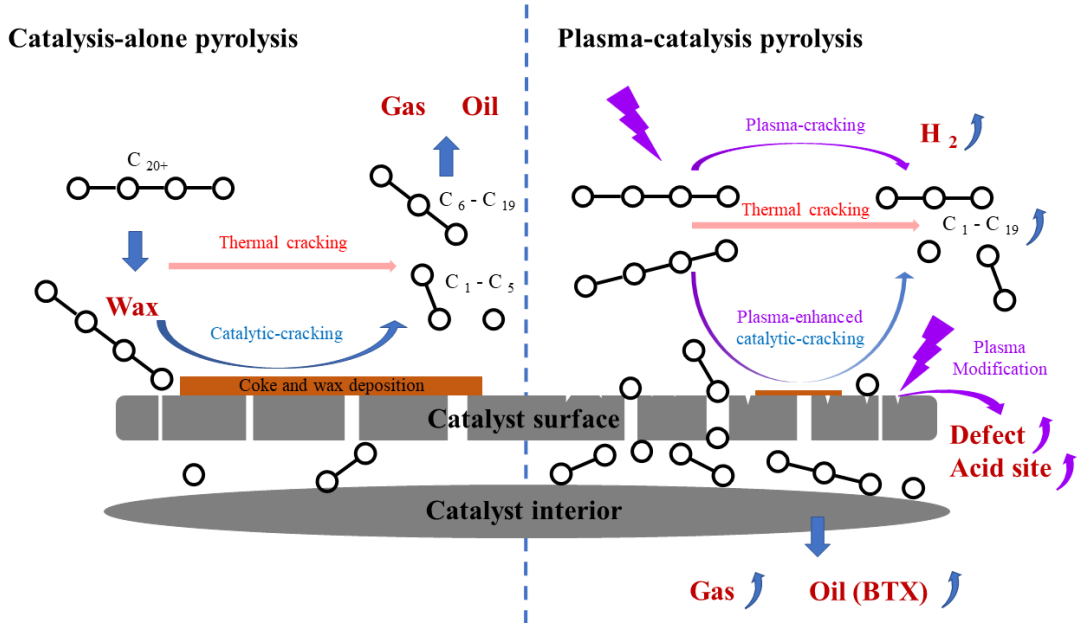

Fig. 12. Synergy mechanism of plasma-catalysis pyrolysis compared with conventional catalytic pyrolysis.

3.3.3. Discussion about practical implications, limitations and future direction

Plasma-catalytic pyrolysis has demonstrated great potential to solve the major problems of wax formation (Lu et al., 2012), low selectivity of target products (Miandad et al., 2016) and catalyst deactivation (Vollmer et al., 2021) in the catalytic conversion of plastics into higher-value fuels and chemicals.

To further identify the economic viability of this process, the cost breakdown of conventional catalytic pyrolysis (without plasma) and plasma-catalytic pyrolysis process has been compared. The annual costs of catalytic pyrolysis mainly include feedstocks, catalyst, electricity, water and labor, as shown in **Table 2**. The cost and amount of feedstocks, water and labor are referenced from the literature (Cai et al., 2021; Sunwen Xia, 2018; Yuxin, 2021). The amount of ZSM-5 and electricity were calculated according to the experimental method.

Catalysts accounted for a major cost in the conventional catalytic pyrolysis process, while catalysts and electricity are the major costs in the plasma-catalytic pyrolysis process. The introduction of plasma led to a nearly 4-fold increase in the cost of electricity but a reduction in the amount of catalyst by more than 10 times. The significant increase in electricity cost caused by plasma might be a barrier limiting the potential commercialization of the plasma process. The cost of plastic and water would not be affected by plasma, while the labor cost might increase due to the additional

equipment management. Overall, plasma resulted in a nearly 77% reduction in total operational costs, which was attributed to reduced catalyst use. Moreover, plasma improved the quality and yield of oil and gas products, which can greatly enhance the revenue of the products. In summary, a rough estimation based on our experimental studies has shown that plasma-catalytic pyrolysis as an emerging technology is promising for waste plastic recycling.

For prospective insight, the main limitations of the advanced pyrolysis technologies are the process scaling-up and cost control of the plasma-catalytic pyrolysis equipment. DBD plasma reactors are challenging to enlarge with the expansion of the pyrolysis chamber due to the limited discharge gap. In the early stage of industrial application, the pretreatment and posttreatment of the catalyst by the plasma modification is a process that is easier to achieve and also enhance the catalytic process to a certain extent. In addition, the feasibility of other feedstocks and more suitable catalysts should also be evaluated in the process of ongoing research.

Table 2 The comparison of operating cost between conventional catalytic pyrolysis and plasma-catalytic pyrolysis

Item	Unit price	Amount		Cost		Proportion	
		Without plasma	With plasma	Without plasma (USD)	With plasma (USD)	Without plasma	With plasma
Plastics	60 (USD/t)	100 (t)	100 (t)	6,000	6,000	0.36%	1.54%
ZSM-5	7853 (USD/t)	200 (t)	18 (t)	1,570,600	141,354	94.03%	36.25%
Electricity	0.1133 (USD/kWh)	426,573 (kWh)	1,676,573 (kWh)	48,330.7	189,955.7	2.89%	48.72%
Water	0.0756	120 (t)	120 (t)	9,072	9,072	0.54%	2.33%

	(USD/t)						
Salary	3,626.4 (USD/y)	10 (workers)	12 (workers)	36,264	43,516.8	2.17%	11.16%
Total				1,670,266.7	389,898.5		

4. Conclusions

Plasma-catalytic pyrolysis as an emerging pyrolysis technology has shown great potential for solving the major problems in the conversion of waste plastic into higher-value fuels and chemicals. The coupling of plasma-catalysis and pyrolysis generated more gas products such as H_2 and CH_4 and enhanced the selectivity of BTX and catalyst stability whilst completely eliminating the formation of wax. The results showed that the plasma modification of the ZSM-5 catalyst enhanced the number of acidic sites of the catalyst, while plasma pre-cracking of volatiles greatly enhanced the catalytic performance, resulting in the formation of less coke deposition on the catalyst. This work shed light on the super function of plasma on enhancing catalytic pyrolysis performance, a process that is expected to reduce the cost of catalyst as well as improve the quality of products during plastics utilization.

Conflicts of interest

There are no conflicts to declare.

Acknowledgements

The authors wish to express sincere thanks for the financial support from the National Natural Science Foundation of China (51976065), National Science Fund for Distinguished Young Scholars program (52125601). The authors are also grateful for

the assistance on the catalyst's analysis provided by the Analytical and Testing Center in Huazhong University of Science & Technology (http://atc.hust.edu.cn), Wuhan 430074, China. X. Tu acknowledges the funding from the Royal Society Newton Advanced Fellowship (No. NAF/R1180230) and British Council Newton Fund Institutional Links Grant (No. 623389161).

References

Adyel, T.M., 2020. Accumulation of plastic waste during COVID-19. Science 369 (6509), 1314-1315.

Aguado, R., Olazar, M., San Jose, M.J., Gaisan, B., Bilbao, J., 2002. Wax formation in the pyrolysis of polyolefins in a conical spouted bed reactor. Energy & Fuels 16 (6), 1429-1437.

Ahmed, S., Aitani, A., Rahman, F., Al-Dawood, A., Al-Muhaish, F., 2009. Decomposition of hydrocarbons to hydrogen and carbon. Applied Catalysis A: General 359 (1), 1-24.

Blanquet, E., Nahil, M.A., Williams, P.T., 2019. Enhanced hydrogen-rich gas production from waste biomass using pyrolysis with non-thermal plasma-catalysis. Catalysis Today 337, 216-224.

Cai, N., Xia, S.W., Li, X.Q., Sun, L., Bartocci, P., Fantozzi, F., Zhang, H.Z., Chen, H.P., Williams, P.T., Yang, H.P., 2021. Influence of the ratio of Fe/Al_2O_3 on waste polypropylene pyrolysis for high value-added products. Journal of Cleaner Production 315, 114819.

Che, Q., Yang, M., Wang, X., Yang, Q., Williams, L.R., Yang, H., Zou, J., Zeng, K., Zhu, Y., Chen, Y., Chen, H., 2019. Influence of physicochemical properties of metal modified ZSM-5 catalyst on benzene, toluene and xylene production from biomass catalytic pyrolysis. Bioresource Technology 278, 248-254.

Chen, Y., Yang, H., Wang, X., Zhang, S., Chen, H., 2012. Biomass-based pyrolytic polygeneration system on cotton stalk pyrolysis: Influence of temperature. Bioresource Technology, 107, 411-418.

Deminsky, M., Jivotov, V., Potapkin, B., Rusanov, V., 2002. Plasma-assisted production of hydrogen from hydrocarbons. Pure and Applied Chemistry 74 (3), 413-418.

Diaz-Silvarrey, L.S., Zhang, K., Phan, A.N., 2018. Monomer recovery through advanced pyrolysis of waste high density polyethylene (HDPE). Green Chemistry 20 (8), 1813-1823.

Epping, J.D., Chmelka, B.F., 2006. Nucleation and growth of zeolites and inorganic mesoporous solids: Molecular insights from magnetic resonance spectroscopy. Current Opinion in Colloid & Interface Science 11 (2), 81-117.

George, M., Pandey, A.K., Rahim, N.A., Tyagi, V.V., Shahabuddin, S., Saidur, R., 2020. Long-term thermophysical behavior of paraffin wax and paraffin wax/polyaniline (PANI) composite phase change materials. Journal of Energy Storage 31, 101568.

Geyer, R., Jambeck, J.R., Law, K.L., 2017. Production, use, and fate of all plastics ever made. Science Advances 3 (7), 5.

Guo, Y.F., Ye, D.Q., Chen, K.F., He, J.C., Chen, W.L., 2006. Toluene decomposition using a wire-plate dielectric barrier discharge reactor with manganese oxide catalyst in situ. Journal of Molecular Catalysis A: Chemical 245 (1), 93-100.

Huang, H., Tang, L., 2007. Treatment of organic waste using thermal plasma pyrolysis technology. Energy Conversion and Management 48 (4), 1331-1337.

643 Kameshima, S., Tamura, K., Ishibashi, Y., Nozaki, T., 2015. Pulsed dry methane reforming in plasma-
644 enhanced catalytic reaction. Catalysis Today 256, 67-75.
645 Kruse, T.M., Wong, H.-W., Broadbelt, L.J., 2003. Mechanistic modeling of polymer pyrolysis:
646 polypropylene. Macromolecules 36 (25), 9594-9607.
647 Kwak, J.H., Peden, C.H.F., Szanyi, J., 2006. Non-thermal plasma-assisted NO_x reduction over Na-Y
648 zeolites: the promotional effect of acid sites. Catalysis Letters 109 (1-2), 1-6.
649 Lippmaa, E.T., Maegi, M., Samoson, A.V., Tarmak, M., Engelhardt, G., 1981. Investigation of the
650 structure of zeolites by solid-state high-resolution ^{29}Si NMR spectroscopy. Journal of the American
651 Chemical Society 103 (17), 4992-4996.
652 Liu, C.J., Yu, K.L., Zhang, Y.P., Zhu, X.L., He, F., Eliasson, B., 2004. Characterization of plasma treated
653 Pd/HZSM-5 catalyst for methane combustion. Applied Catalysis B-Environmental 47 (2), 95-100.
654 Lopez-Urionabarrenechea, A., de Marco, I., Caballero, B.M., Laresgoiti, M.F., Adrados, A., Aranzabal,
655 A., 2011. Catalytic pyrolysis of plastic wastes with two different types of catalysts: ZSM-5 zeolite and
656 Red Mud. Applied Catalysis B-Environmental 104 (3-4), 211-219.
657 Lopez, G., Artetxe, M., Amutio, M., Bilbao, J., Olazar, M., 2017. Thermochemical routes for the
658 valorization of waste polyolefinic plastics to produce fuels and chemicals. A review. Renewable and
659 Sustainable Energy Reviews 73, 346-368.
660 Lu, Y., Huang, Z., Hoffmann, R., Amundsen, L., Fogler, H.S., 2012. Counterintuitive effects of the oil
661 flow rate on wax deposition. Energy & Fuels 26 (7), 4091-4097.
662 Miandad, R., Barakat, M.A., Aburiazaiza, A.S., Rehan, M., Nizami, A.S., 2016. Catalytic pyrolysis of
663 plastic waste: A review. Process Safety and Environmental Protection 102, 822-838.
664 Muhammad, C., Onwudili, J.A., Williams, P.T., 2015. Thermal degradation of real-world waste plastics
665 and simulated mixed plastics in a two-stage pyrolysis-catalysis reactor for fuel production. Energy &
666 Fuels 29 (4),2601-2609.
667 Neyts, E.C., Ostrikov, K.K., Sunkara, M.K., Bogaerts, A., 2015. Plasma catalysis: synergistic effects at
668 the nanoscale. Chemical Reviews 115 (24) 13408-13446.
669 Oasmaa, A., Qureshi, M.S., Pihkola, H., Deviatkin, I., Mannila, J., Tenhunen, A., Minkkinen, H.,
670 Pohjakallio, M., Laine-Ylijoki, J., 2020. Pyrolysis of plastic waste: Opportunities and challenges. Journal
671 of Analytical and Applied Pyrolysis 152, 104804.
672 Prata, J.C., Silva, A.L.P., Walker, T.R., Duarte, A.C., Rocha-Santos, T., 2020. COVID-19 pandemic
673 repercussions on the use and management of plastics. Environmental Science & Technology 54 (13),
674 7760-7765.
675 Ravi, M., Sushkevich, V.L., van Bokhoven, J.A., 2020. Towards a better understanding of Lewis acidic
676 aluminium in zeolites. Nature Materials 19 (10), 1047-1056.
677 Xia, S.W., Xiao, H.Y., Liu, M., Chen, Y.Q., Yang, H.P., Chen, H.P., 2018. Pyrolysis behavior and
678 economics analysis of the biomass pyrolytic polygeneration of forest farming waste. Bioresource
679 Technology 270, 189–197
680 Vogt, Weckhuysen, 2015. Fluid catalytic cracking: recent developments on the grand old lady of zeolite
681 catalysis. Chemical Society Reviews 44, 7342.
682 Vollmer, I., Jenks, M.J.F., Gonzalez, R.M., Meirer, F., Weckhuysen, B.M., 2021. Plastic waste conversion
683 over a refinery waste catalyst. Angewandte Chemie-International Edition 60 (29), 16101-16108.
684 Weckhuysen, B.M., 2020. Creating value from plastic waste. Science 370 (6515), 400-401.
685 Xia, S.W., Li, K.X., Xiao, H.Y., Cai, N., Dong, Z.G., Xu, C., Chen, Y.Q., Yang, H.P., Tu, X., Chen, H.P.,
686 2019. Pyrolysis of Chinese chestnut shells: Effects of temperature and Fe presence on product

composition. Bioresource Technology 287, 8.
Xia, S.W., Yang, H.P., Lu, W., Cai, N., Xiao, H.Y., Chen, X., Chen, Y.Q., Wang, X.H., Wang, S.R., Wu, P., Chen, H.P., 2022. Fe-Co based synergistic catalytic graphitization of biomass: Influence of the catalyst type and the pyrolytic temperature. Energy 239, 122262.
Yaneva, Z., Georgieva, N., Pavlov, A., 2016. Low-temperature plasma-modified zeolite vs. natural bulgarian zeolite-comparative physicochemical, spectrophotochemical and fourier transform infrared spectoscopy studies. Macedonian Journal of Chemistry and Chemical Engineering 35 (1), 97-105.
Yao, D., Wang, C.-H., 2020. Pyrolysis and in-line catalytic decomposition of polypropylene to carbon nanomaterials and hydrogen over Fe- and Ni-based catalysts. Applied Energy 265, 114819.
Yao, D., Yang, H., Chen, H., Williams, P.T., 2018. Co-precipitation, impregnation and so-gel preparation of Ni catalysts for pyrolysis-catalytic steam reforming of waste plastics. Applied Catalysis B: Environmental 239, 565-577.
Yuxin, J., 2021. Study on the effect of additives on the characteristics of biochar prepared by pyrolysis of biogas residue and the improvement of preparation process [D]. Guizhou Minzu University. DOI:10.27807/d.cnki.cgzmz.2021.000309.
Zeng, Y.X., Wang, L., Wu, C.F., Wang, J.Q., Shen, B.X., Tu, X., 2018. Low temperature reforming of biogas over K-, Mg- and Ce-promoted Ni/Al_2O_3 catalysts for the production of hydrogen rich syngas: Understanding the plasma-catalytic synergy. Applied Catalysis B-Environmental 224, 469-478.
Zhang, X., Lei, H., Yadavalli, G., Zhu, L., Wei, Y., Liu, Y., 2015. Gasoline-range hydrocarbons produced from microwave-induced pyrolysis of low-density polyethylene over ZSM-5. Fuel 144, 33-42.
Zheng, A.Q., Zhao, Z.L., Chang, S., Huang, Z., Wu, H.X., Wang, X.B., He, F., Li, H.B., 2014. Effect of crystal size of ZSM-5 on the aromatic yield and selectivity from catalytic fast pyrolysis of biomass. Journal of Molecular Catalysis A: Chemical 383, 23-30.
Zhu, F., Zhang, H., Yang, H., Yan, J., Li, X., Tu, X., 2020. Plasma reforming of tar model compound in a rotating gliding arc reactor: Understanding the effects of CO_2 and H_2O addition. Fuel 259, 116271.